Numerical Assessment of Frictional Heating in Sliding Bearings for Seismic Isolation

VIRGINIO QUAGLINI, MASSIMILIANO BOCCIARELLI, EMANUELE GANDELLI, and PAOLO DUBINI

Politecnico di Milano, Department of Architecture, Built Environment and Construction Engineering A.B.C., Milano, Italy

1. Introduction

The Curved Surface Slider (CSS), also known as Friction Pendulum System (FPS) [Zayas *et al.*, 1987, 1990], is today a well-established seismic hardware for base isolation of buildings and structures, regulated in the most recent American [ASCE/SEI 7-10, 2010; AASHTO, 2010] and European [EN 15129, 2009] standards on antiseismic devices. Among the main features of the CSS there are the compact design and smaller dimensions than seismic rubber isolators with same load and displacement capacity, the period of vibration independent of the mass of the isolated superstructure, and the absence of torsional effects in presence of asymmetric buildings.

The dynamic characteristics of the isolation unit are expressed by the effective period of vibration T_{eff}, the effective stiffness, K_{eff}, defined as the ratio of the difference in maximum and minimum lateral forces to the difference in maximum and minimum lateral displacements, and the effective damping ξ_{eff}. For the CSS isolator these properties are governed by the equivalent radius R and the coefficient of friction μ of the curved surfaces, according to the following relations [Zayas *et al.*, 1990]:

Received 8 August 2013; accepted 10 May 2014.

Address correspondence to Virginio Quaglini, Politecnico di Milano, Department of Architecture, Built Environment and Construction Engineering A.B.C. Piazza Leonardo da Vinci 32 20133, Milano, Italy. E-mail: virginio.quaglini@polimi.it

$$T_{eff} = 2\pi\sqrt{\frac{N}{K_{eff}\cdot g}} = 2\pi\sqrt{\frac{1}{1+\frac{\mu\cdot R}{A}}\cdot\frac{R}{g}} \tag{1}$$

$$K_{eff} = \left(1+\frac{\mu\cdot R}{A}\right)\cdot\frac{N}{R} \tag{2}$$

$$\xi_{eff} = \frac{2}{\pi}\frac{\mu}{\mu+\frac{A}{R}}, \tag{3}$$

where A is the displacement amplitude, g is the acceleration of gravity, and N is the vertical load acting on the isolator.

The sliding surfaces of the isolator usually consist of a pad of a self-lubricant material rubbing onto a steel concave plate; the relevant friction force is aimed at promoting dissipation of seismic energy during the earthquake, but must not restrain slow service movements like, e.g., those produced by thermal effects. Durability of the pad material is fundamental to decide whether the isolator is capable of sustaining high velocities and a large amount of movements without any deterioration. After the Friction Pendulum System was firstly introduced at the end of the '80s [Mokha *et al.*, 1991, 1996], a number of self-lubricant materials like filled PolyTetraFluorEthylene (PTFE) and PTFE compounds, Ultra High Molecular Weight PolyEthylene (UHMWPE) and other thermoplastics have been proposed as bearing materials [Constantinou *et al.*, 1993, 2007; Tsai *et al.*, 2006; Tsopelas and Constantinou, 1994; Braun, 2009; Quaglini *et al.*, 2012]. However, the choice of a material suitable for the operation of CSS isolators is not trivial, and in this respect, a major issue is associated to the generation of heat occurring under large friction forces and high velocities [Constantinou *et al.*, 2007; Wolff, 1999; Drozdov *et al.*, 2008]. Most of the mechanical work done against friction forces to maintain sliding between the pad and its mating surface is converted into heat, producing temperature rise, usually of short duration and therefore called "flash temperature", at the interface [Stachowiak and Batchelor, 2005]. High flash temperatures developed under strong or long duration earthquakes can promote oxidation of the steel surface, affect the local geometry through thermal expansion effects, and even cause surface melting, accelerating the wear of the sliding material.

The thermal state of sliding isolation systems has been investigated in the recent years in analytical and finite element studies. Constantinou *et al.* [2007] presented an analytical model to calculate the average temperature rise at the contact surface and at small depths below the surface of a FPS. For a large FP bearing designed to carry a gravity load of more than 75 MN in an offshore platform [Clarke *et al.*, 2005] subjected to biaxial motion at velocities up to 0.8 m/s, peak temperatures as high as 400°C were predicted. Drozdov *et al.* [2008] performed a numerical study to evaluate the steady-state temperature in a spherical bearing under different loading histories, underlining the importance of estimating the temperature profile inside the friction pendulum in order to choose suitable self-lubricating materials according to their thermal stability.

All these studies focused on the prediction of the temperature rise as a factor for the potential deterioration of the surfaces, but did not address the effect of temperature on the coefficient of friction. Substantial heating can promote local melting of the bearing material, reducing considerably the coefficient of friction, e.g., in isolators with PTFE/steel interface Mosqueda *et al.* [2004] measured a decrease in friction on the order of 20% after 3 cycles of loading at peak velocities larger than 127 mm/s, and similar results related to self-heating of the PTFE pad were found in small scale tests by Dolce *et al.* [2005]. The development of reliable numerical approaches for the analysis of sliding isolation systems

can therefore assist preliminary studies for the selection of bearing materials, reserving prototype tests to the final evaluation of the device.

The assessment of the influence of temperature on the dynamic characteristics of the isolation system is also important in establishing property modification factors for the coefficient of friction that are required for Upper and Lower Bound analyses by design codes. However, due to few experimental background, modification factors accounting for high temperatures developed at the sliding surface by frictional heating have not yet been established, and the modification factors recommended in the current standards [AASHTO, 2010; EN 1337-2, 2004] regulate the influence of the environmental temperature only, which can be considerably different from the flash temperature developed at the sliding surface during the earthquake.

The manuscript proposes a computational approach for the investigation of frictional heating in CSS isolators by means of coupled thermal–mechanical finite element analyses. The numerical procedure is illustrated for a typical CSS design. The generation of frictional heat is reproduced in the numerical model by means of a heat source with local intensity dependent on the coefficient of friction, the relative speed and the contact pressure at the sliding surfaces. The heat flux and temperature histories are calculated step by step by the finite element model: a custom algorithm iteratively adjusts the coefficient of friction on the current surface temperature and sliding velocity, and this value is used to update the heat flux at the next calculation step. The resisting force of the isolator is finally predicted based on the current value of friction. The finite element formulation was validated based on temperature and force–displacement histories measured in laboratory tests on a full scale isolator. The numerical study specifically addresses the assessment of the surface temperature developed during sliding, with regards to both the thermal stability of the bearing materials, and the influence on the stiffness and damping characteristics of the isolator.

2. Description of the Curved Surface Slider

The procedure is illustrated with reference to a Curved Surfaces Slider with one pair of curved sliding surfaces and a spherical articulation (Fig. 1), designed for the seismic isolation of high speed railway viaducts in the Marmara region, each viaduct being 1020 m long and composed of 31 spans [Sartori, 2012]. The main parts of the CSS unit are the sliding plate, the pivot, the articulation base (or basement), and two pads: the sliding pad mating the concave surface of the sliding plate and the rotation pad positioned in between

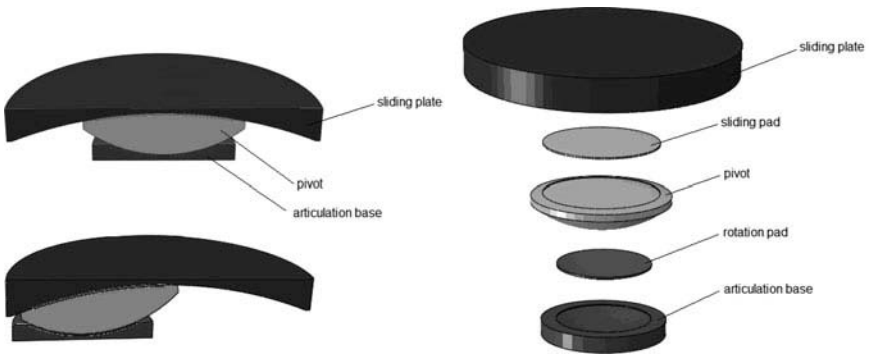

FIGURE 1 Sketch of the CSS unit: operation principle (left) and detail of its main component parts (right).

the pivot and the basement. The sliding plate, basement, and pivot are made of carbon steel, with the surfaces of the sliding plate and of the pivot mating the pads covered with a thin (2 mm) overlay of polished stainless steel. The radii of curvature are 1650 mm for the sliding surface of the sliding plate and 530 mm for the spherical articulation, respectively.

Two different self-lubricating materials are employed for the pads. The material of the rotation pad is a low friction material used to minimize the frictional resistance at the spherical articulation. The bearing material of the sliding pad is a PTFE compound with a design kinetic coefficient of friction at high velocity of 0.12 and variation limits between 0.04 and 0.165 within the ranges of pressure and velocity considered in the study [Quaglini *et al.*, 2012]. The diameters of the two pads are 456 mm (rotation pad) and 560 mm (sliding pad), respectively, and the thickness of both of them is 7 mm.

A specimen of the CSS isolator was tested at the experimental facility of the Eucentre laboratory in Pavia, Italy, using the Bearing Tester System, a custom biaxial system for full-scale testing of bearings and isolation devices [Calvi *et al.*, 2005; Lanese *et al.*, 2012].

A compressive vertical load of 4500 kN was applied to the specimen, and four cycles of sinusoidal motion with amplitude of either 85 mm (Test1) or 170 mm (Test2), and period of 2.13 seconds, were performed. It was checked that during the cycles the test equipment was able to accommodate the vertical displacement that the concave sliding plate undergoes under horizontal movement, maintaining the vertical load nearly constant: experimental fluctuations in vertical load were within plus/minus ten per cent of the rated set-point value for more than 95% of the total stroke (Fig. 2). The load and displacement histories were recorded and processed to remove the inertial forces due to the acceleration of the testing equipment at the first start and at the reversals of motion. The hysteretic load–displacement curves of the isolator were then plotted and the stiffness and energy dissipated by the CSS unit were calculated at each cycle.

The ambient temperature of the laboratory at the beginning of the tests was 23°C. Thermocouples were embedded into the sliding plate of the CSS (Fig. 3), with their probes in contact with the back of the austenitic steel overlay at a depth of 2 mm from the sliding surface, and the temperature at the overlay was continuously recorded throughout the tests. N-type thermocouples with a wire diameter of 0.20 mm were utilized in an attempt to increase the sensitivity of the instrument and obtain reliable measurements of temperature histories under conditions of high speed motion.

3. Thermal–Mechanical Analysis

3.1. Finite Element Model

A three-dimensional geometrical model of the CSS unit was created in the commercial code ABAQUS v. 6.13 (Dassault Systèmes Simulia Corp., Providence, RI) and subdivided in a mesh of three dimensional finite elements (Fig. 4). Either linear and wedge thermal-mechanical coupled hexaedrical elements, type C3D8T and C3D6T, respectively, with four degrees of freedom (displacement components along three directions and temperature) at each node, were used. Details of the mesh are reported in Table 1. Mechanical and thermal properties were assigned to the materials of the isolator in accordance with Table 2.

During the movement of the bearing, frictional heating is generated at the interface between the sliding pad and the sliding plate and, to a lesser extent, at the spherical articulation. Following Constantinou *et al.* [2007], at each interface a surface heat source spread all over the contour area of the pad is assumed, which produces a local heat flux of intensity

$$q = \mu \cdot p \cdot V, \tag{4}$$

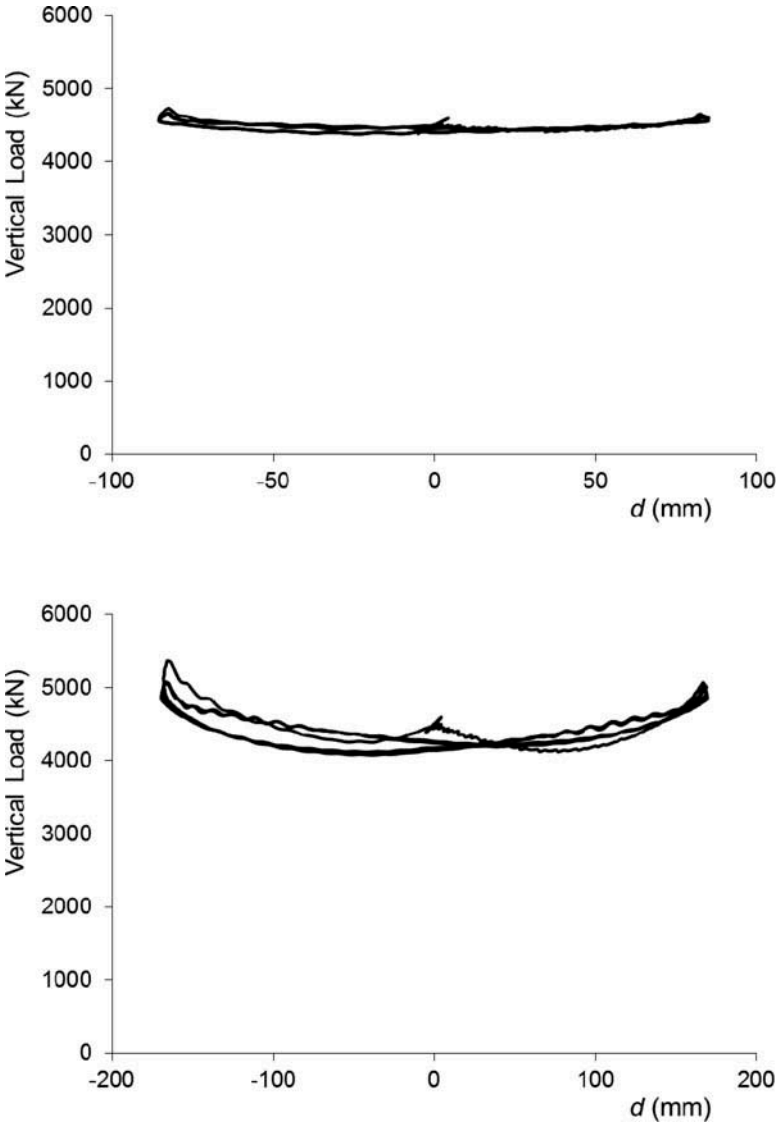

FIGURE 2 Records of the vertical load applied by the testing equipment to the CSS specimen during Test1 (above) and Test2 (below).

where μ is the coefficient of friction, p is the contact pressure, and V is the sliding velocity.

The coefficient of friction of the sliding pad μ was formulated in a custom subroutine as an explicit function of the surface velocity and temperature.

1. An isotropic velocity-dependent friction model was defined with a smooth transition zone from the low velocity to the high velocity regime regulated by an exponential function, adapted from Constantinou *et al.* [1990]:

$$\begin{aligned}\mu_{\text{vel}} &= f_{k2} - (f_{k2} - f_{k1}) \cdot exp(-\alpha_1 \cdot V) \\ &+ (f_{st} - f_{k1}) \cdot exp(-\alpha_2 \cdot V) \cdot \frac{|sign(V) - sign(d)|}{2},\end{aligned} \tag{5}$$

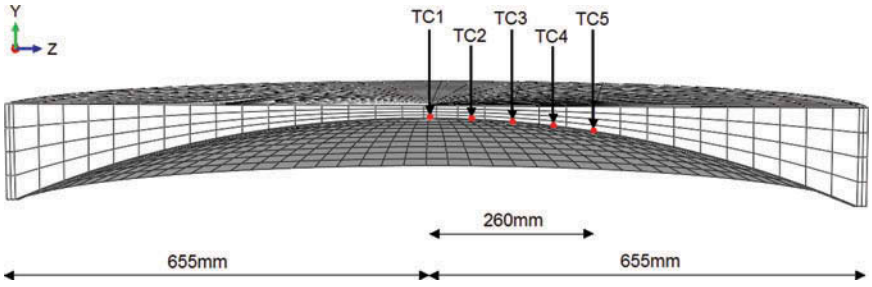

FIGURE 3 Position of thermocouples embedded into the concave sliding plate of the CSS unit. Five thermocouples, equally spaced by 65 mm, were aligned perpendicularly (along the Z axis) to the direction of displacement of the CSS bearing (along the X axis).

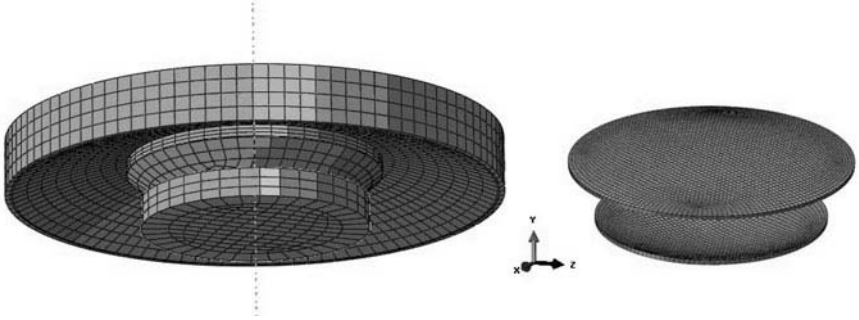

FIGURE 4 Finite element mesh of the CSS unit: complete bearing (left) and detail of the sliding and rotation pads (right).

TABLE 1 Size of the finite element mesh

	Elements (#)		
Component	C3D8T	C3D6T	Nodes (#)
sliding plate	7636	2512	11026
sliding pad	5216	–	6815
pivot	960	–	1396
rotation pad	3840	–	5045
articulation base	340	–	585
Total	17992	2512	24867

where f_{k1} is the kinetic coefficient of friction at low velocity, f_{k2} is the kinetic coefficient of friction at high velocity, f_{st} is the static coefficient of friction that opposes the initiation of sliding when velocity is zero (e.g., at breakaway and at motion reversals), α_1 is a parameter regulating the increase in kinetic friction with velocity, α_2 is a parameter regulating the transition from the static to the kinetic friction regime, V is the velocity variable, and d is the displacement variable. The term $|sign(V) - sign(d)|$ is not zero only when the sliding pad reverses its motion after a stop, like in cyclic displacement histories.

TABLE 2 Material properties

	Mechanical		Thermal	
Material	Elastic modulus (MPa)	Poisson's ratio (-)	Conductivity (mW/(mm K))	Specific heat (J/(kg K))
carbon steel	$2.09{\cdot}10^5$	0.30	53.7	$4.9{\cdot}10^5$
stainless steel	$1.96{\cdot}10^5$	0.30	16.0	$5.0{\cdot}10^5$
sliding pad	$8.00{\cdot}10^2$	0.45	0.65	$1.1{\cdot}10^6$
rotation pad	$2.80{\cdot}10^3$	0.45	0.25	$1.7{\cdot}10^6$

TABLE 3 Parameters of the temperature and velocity-explicit friction model

Parameter		
f_{k1}	0.040	
f_{k2}	0.120	
f_{st}	0.165	
α_1	0.015	$(\text{mm/s})^{-1}$
α_2	0.250	$(\text{mm/s})^{-1}$
β	0.005	$^{\circ}\text{C}^{-1}$

2. It was assumed that the coefficient of friction calculated by Eq. (5) decays exponentially as the temperature increases according to the formula

$$\mu = \mu_{\text{vel}} \cdot exp(-\beta \cdot \theta), \tag{6}$$

where β is the decay coefficient and θ is the temperature variable.

The set of parameters assumed in the analyses is reported in Table 3. The parameters of the velocity–dependent friction function μ_{vel}, Eq. (5), were calibrated on the experimental force–displacement curve of the CSS unit recorded at the first cycle of Test2, while the temperature decay parameter β of Eq. (6) was determined in friction tests performed on material specimens (75 mm diameter) at temperatures between 20°C and 100°C. Test2 was chosen for calibrating the kinetic friction parameters as higher velocities were produced than in Test1.

At the spherical articulation a constant value of the coefficient of friction of 0.005 was taken, neglecting the effect of temperature due to the small entity of the relevant heat flux and the expected temperature rise.

Both at the sliding interface and at the spherical articulation, the generated heat flux q is partitioned into two fluxes $q_1 = K \cdot q$ supplied to the steel part, and $q_2 = (1 - K) \cdot q$ supplied to the polymeric pad, where K is the heat separation factor that depends on the thermal properties and geometry of the bodies in contact.

Mechanical and thermal boundary conditions were set as follows.

1. A constant vertical load is applied to the CSS, uniformly distributed on the upper surface of the sliding plate.
2. A horizontal movement is prescribed to the sliding plate, while the basement is kept fixed.
3. While subjected to the prescribed horizontal movement, due to the rotation of the spherical articulation, the sliding plate has a vertical movement as well; constrains

are introduced to keep the top surface of the sliding plate parallel to the ground surface of the basement.
4. A uniform temperature θ_0 is set for the whole CSS at the beginning of the analysis.
5. The temperature on the top and ground surfaces of the CSS holds constant at the initial value θ_0 during the whole duration of the analysis, simulating the installation of the CSS unit in a massive structure or in the testing machine where the temperature rise is zero at some distance from the moving interfaces.
6. Conductivity heat transmission is allowed at both the sliding and the rotation interfaces.
7. The lateral walls of the isolator are adiabatic; this assumption is valid for short-time intervals which allow for the neglecting of energy losses by radiation and convection.

The coupled thermal-mechanical problem in the physical model is described by a system of partial differential equations with the above boundaries conditions, formulated in terms of either known temperatures or fluxes [Incropera *et al.*, 2006] and displacements or loads. Using the finite element approach a numerical solution of the heat balance equation, together with the equations governing the mechanical problem, in terms of nodal temperatures and displacements was calculated by the computer code ABAQUS [2013].

3.2. Thermal Calibration of the Model

To determine the heat separation factor K at each interface, a preliminary analysis was carried out, where the sliding plate was kept fixed with respect to the basement and heat generation was introduced into the model by means of two arbitrary heat sources of constant intensity located at the interfaces of the sliding plate and of the articulation base.

A vertical load of 4500 kN was applied to the model to generate contact at the interfaces and allow thermal conductance. Numerical integration of the heat balance equation with known temperature at the boundary surfaces of the isolator provided the heat fluxes within the CSS unit. Table 4 shows that, owing to the poor thermal conductivity of the materials of the two pads, almost the totality of frictional heat generated at each interface enters the surface of the steel part: the heat separation factor is on the order of 99% at the sliding plate and 95% at the pivot.

3.3. Numerical Analyses

In order to compare numerical predictions for the CSS unit with experimental data, the laboratory tests described in Sec. 2 were reproduced with the finite element model.

Two tests were numerically simulated, in accordance with the conditions reported in Table 5. The simulated time duration of each analysis was 8.52 s, corresponding to the four loading cycles performed in the laboratory tests.

TABLE 4 Calibration analysis: average nodal heat fluxes at the interfaces

Interface		nodal heat flux (mW/mm^2)
sliding plate/pivot	q_1 (to the sliding plate)	6.27
	q_2 (to the sliding pad)	0.09
pivot/basement	q_1 (to the pivot)	0.61
	q_2 (to the rotation pad)	0.03

TABLE 5 Test conditions

Parameter		Test1	Test2
vertical load	N	4500 kN	4500 kN
initial temperature	θ_0	23°C	23°C
displacement amplitude	A	85 mm	170 mm
period	T	2.13 s	2.13 s
circular frequency	ω	0.94 rad/s	0.94 rad/s
average sliding speed	V_a	159.6 mm/s	319.2 mm/s
number of cycles	n	4	4

The isolator was subjected to a vertical load of constant intensity $N = 4500$ kN. An unidirectional movement d was applied to the sliding plate according to the waveform

$$d(t) = \tfrac{A}{2} \cdot [1 - \cos(2\omega \cdot \mathrm{t})] \qquad \text{for } 0 \le t \le \tfrac{T}{4} \tag{7a}$$

$$d(t) = A \cdot \mathrm{sen}(\omega \cdot \mathrm{t}) \qquad \text{for } \tfrac{T}{4} < t \le n \cdot T\,, \tag{7b}$$

where A is the displacement amplitude, T is the period, t is the time variable, $\omega = 2\pi/T$ is the circular frequency, and n is the cycle number.

The analysis was divided into two consecutive steps, the first corresponding to the movement of the CSS unit from its undeformed configuration ($d = 0$ mm) at time zero to its maximum displacement A at time $T/4$, and the second corresponding to the remaining part of the test. A different waveform was assumed for either step in order to replicate the actual history of loading performed in the experiments. The initial thermal and mechanical conditions of the second step corresponded to the ones calculated at the end of the first step. Since at the start of motion from the reference configuration $d = 0$ mm the term $|sign(V) - sign(d)|$ accounting for the static coefficient of friction was null, in the first step of the analysis in lieu of Eq. (5) the dependence of the coefficient of friction on velocity was expressed by the formula

$$\mu_{\mathrm{vel}} = f_{k2} - (f_{k2} - f_{k1}) \cdot exp(-\alpha_1 \cdot V) + (f_{st} - f_{k1}) \cdot exp(-\alpha_2 \cdot V). \tag{8}$$

The thermal boundary conditions set for the analysis are the flux distribution at the sliding and rotation surfaces and the temperature at the top and ground surfaces of the CSS, as defined in Sec. 3.2. At each interface the energy dissipated by friction is assumed to be totally converted into heat in accordance with Eq. (4), and 99% of the total heat flux directed to the steel component part ($K = 0.99$). The heat balance equation forms again the basis for the thermal analysis and its numerical integration provides the temperature distribution within the isolator. The size of the time increment is self-adjusted by the software between 0.0001 and 0.5 s in order to keep the temperature change at the sliding surface less than 5°C per increment. At each calculation step a sub-routine iteratively adjusts node by node the coefficient of friction of the sliding pad on the current values of surface velocity and temperature according to Eqs. (5) and (6) and feeds it into Eq. (4) to update the generated heat flux q. The software then calculates the contact stresses and relative velocities at the sliding interfaces, which are used to update the heat flow Eq. (4), and the global reaction force of the isolator.

4. Results

4.1. Temperature Rise Histories due to Frictional Heating

The temperature of the sliding pad is the primary interest of the coupled thermo-mechanical analysis. Figure 5 shows the surface temperature history calculated in Test2 (similar

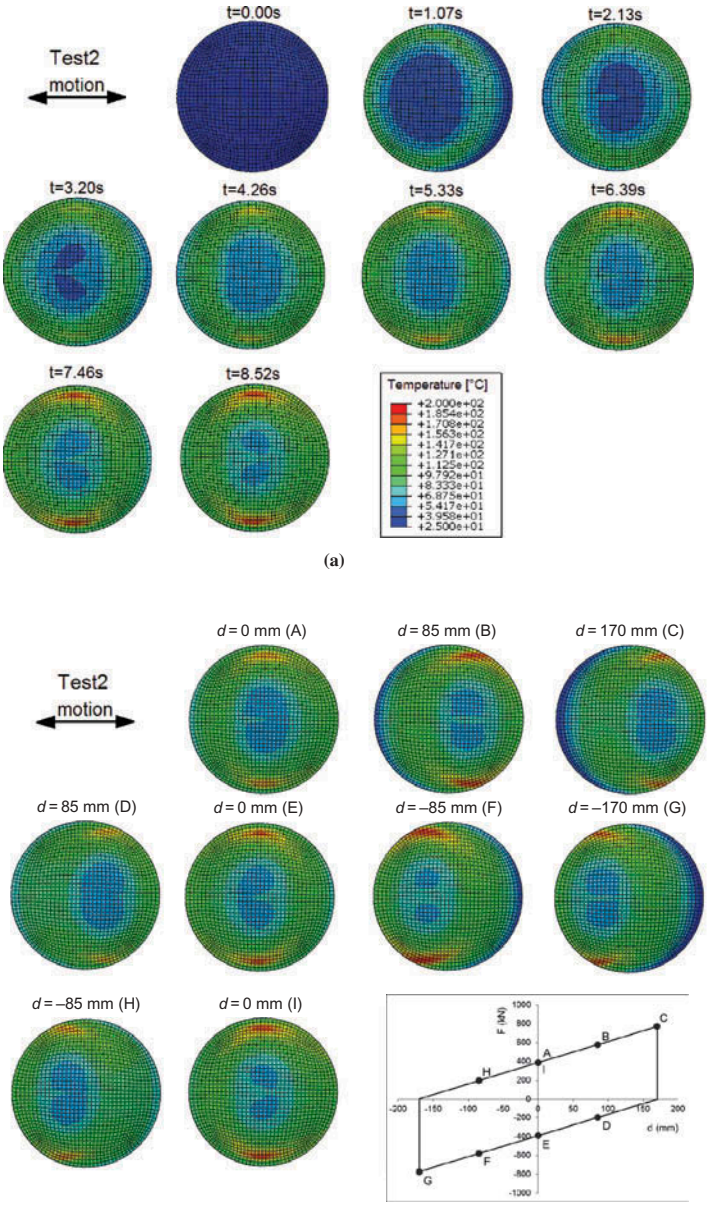

FIGURE 5 Surface temperature of the sliding pad predicted in the finite element analysis: (a) at $d = 0$ mm ("neutral" position of the CSS bearing) over four consecutive cycles of motion in Test2 (period of cycle $T = 2.13$ s); (b) at different values of displacement d of the CSS during the last cycle of Test2.

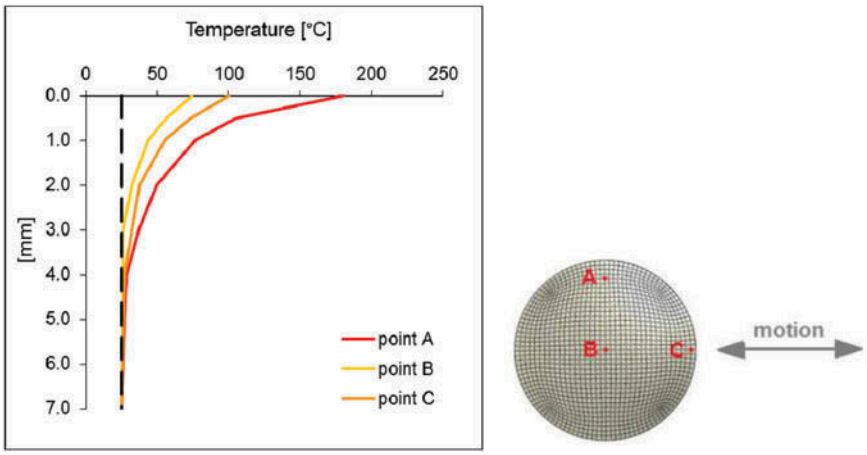

FIGURE 6 Temperature profiles through the thickness of the sliding pad in Test2 at time t = 8.5 seconds.

patterns relevant to Test1 are not reported for brevity). The temperature rise is not uniform, increasing from the center of the pad towards the perimeter (in accordance with the pattern of pressure, as it will be presented in Sec. 4.2), and perpendicularly to the axis of motion. Peak temperatures are predicted to lie in two areas symmetrically placed with respect to the sliding direction, approximately 255–260 mm (90–93% of the radius) from the center of the pad. During the motion of the bearing these two areas of maximum temperature rise shift over the pad surface in the same direction of motion (Fig. 5b). The temperature profile through the thickness of the pad is illustrated in Fig. 6. The temperature rise drops rapidly below the sliding surface, substantially affecting an outer layer of material approximately 1.5 mm thick; at a depth of 2 mm or more the temperature increase can be neglected as the resulting temperature falls within the typical environmental range (less than 50°C).

The temperature at the sliding interface could not be measured in the laboratory tests, but it was possible to record with the embedded thermocouples the temperature histories at a few mm under the surface, on the back of the stainless steel overlay. Figure 7 illustrates the temperature records measured during the laboratory tests by two thermocouples located at the center of the bearing (TC1) and at 260 mm from the center (TC5), perpendicularly to the direction of sliding, in correspondence of the area where peak temperature is predicted on the sliding pad surface. The temperature at the beginning of each test was some degrees higher than the ambient temperature due to heating produced during preliminary calibration of the testing equipment. A continuous increase in temperature was observed, though the temperature rise at the depth of 2 mm was expected to be much less than at the surface, and after 8.5 s a thermal steady-state was not yet attained. Calculated histories are reported in Fig. 7 for two distinct numerical analyses, performed either accounting for the temperature–explicit formulation of the friction coefficient, Eq. (6), or using the velocity-dependent model μ_{vel} of Eqs. (5) and (8) alone. The experimental records are in good agreement with the prediction of the temperature–explicit formulation, especially at TC5 location, while the temperature–independent friction analysis overestimates the temperature rise, with a maximum discrepancy of 16.7°C in Test2 after 4 cycles.

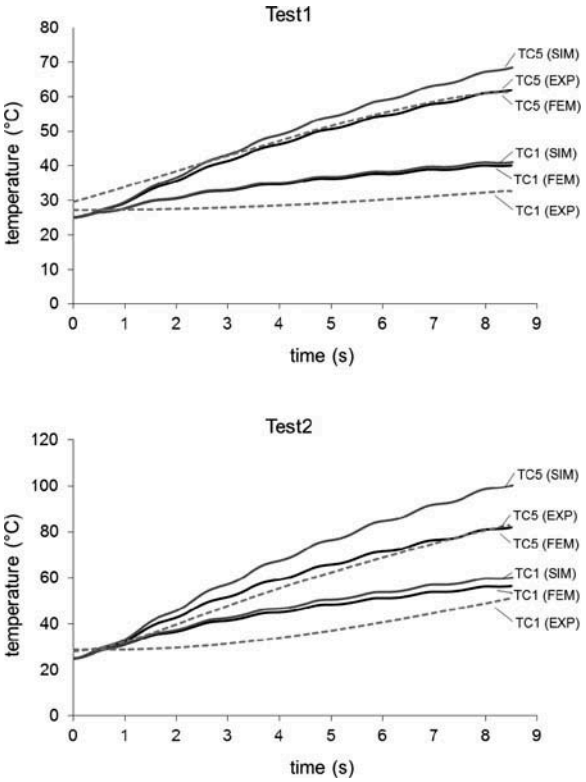

FIGURE 7 Recorded (EXP) and predicted temperature histories in the steel sliding plate, 2 mm below the sliding surface (thermocouple locations: TC1 at the center of the bearing; TC5 in correspondence of the pad surface peak temperature). Numerical analyses performed with either temperature–explicit (FEM) or temperature–independent simplified (SIM) friction formulation.

4.2. Force–Displacement Behavior

The contact stress p on the curved pad surface is not uniform (Fig. 8), increasing radially from the center towards the perimeter due to the curvature of the surface, and along the direction of motion as an effect of both the moment resulting from the eccentricity of the vertical load between the sliding plate and the articulation base and the restraint moment generated by the friction forces on the pivot. The peak stress on the pad is about 45 MPa at rest, without the contribution of the eccentricities generated during the bearing sliding, and increases to about 60 MPa at the maximum displacement amplitude.

Figure 9 compares the hysteretic force–displacement loops predicted in Test2 by the finite element model with the relevant experimental curves (similar results for Test1 are not reported). The agreement between the numerical and the experimental curves is fair, though some deviation occurs in the last branch (from $d = -170$ mm to $d = 0$ mm) of every cycle. From the force–displacement loops the effective stiffness (K_{eff}) and the Energy Dissipated per Cycle (EDC) of the CSS unit are calculated (Fig. 10). As expected, in the laboratory tests both properties show a continuous decrease over the four cycles owing to the effect of temperature rise on the coefficient of friction. This change in properties is well matched in the numerical analyses, with a maximum deviation of about 3% for the stiffness and 4% for

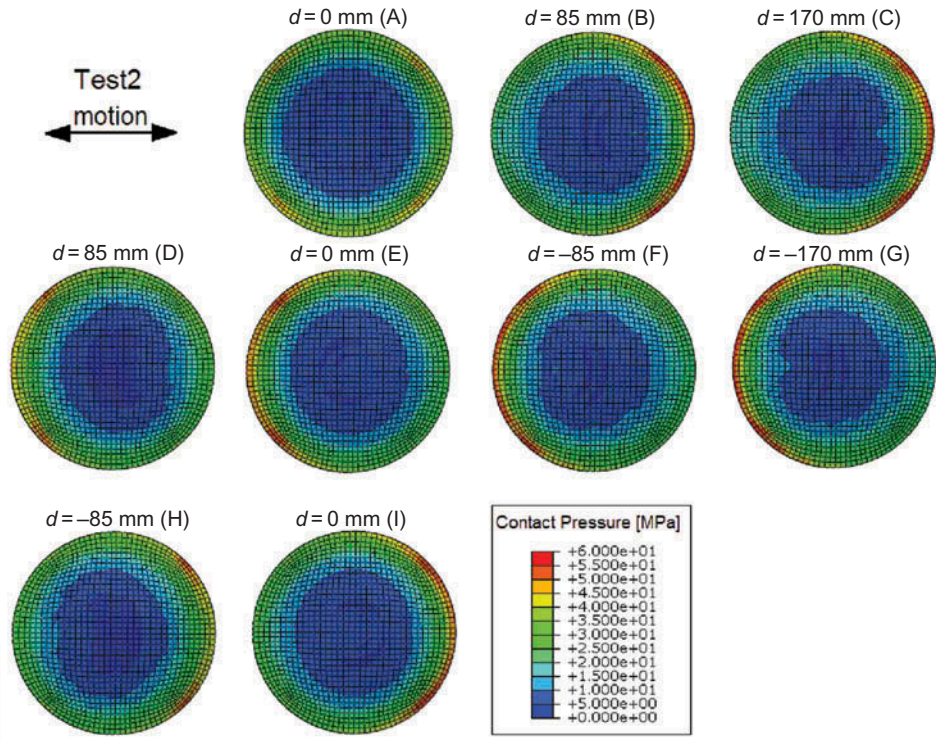

FIGURE 8 Contact stress on the surface of the sliding pad at different values of displacement d of the CSS during Test2 (see Fig. 5b for definition of positions A to I on the hysteretic force-displacement diagram).

the *EDC*. Consistent predictions are obtained for Test1 as well, with maximum deviation of 4.4% for the stiffness and about 7% for the *EDC*.

Figures 9 and 10 report for comparison the predictions of numerical analyses performed using the temperature-independent friction formulation of Eq. (5) for the friction pad. The relevant force-displacement loops systematically overestimate the force measured in the laboratory tests and the model is not able to reproduce the change in dynamic properties of the isolator: the gap between the numerical prediction and the experimental results increases with increasing cycle number, and after four cycles the deviation is +27.5% (K_{eff}) and +60% (*EDC*) in Test1 and +36% (K_{eff}) and +44% (*EDC*) in Test2, respectively (Fig. 10).

5. Discussion

In this article, a numerical procedure for investigating the thermal-mechanical behavior of Curved Surface Sliders by means of finite element analyses has been developed and validated upon experimental unidirectional tests. With respect to previous studies [Constantinou *et al.*, 2007; Drozdov *et al.*, 2008], the procedure carries two main novelties: (a) the thermal generation represented by a heat flux which point by point depends on the local values of contact pressure, sliding velocity, and coefficient of friction of the bearing material, which, in turn, depends on the surface temperature; and (b) the influence of heating on the mechanical response of the device through the temperature–dependent friction model.

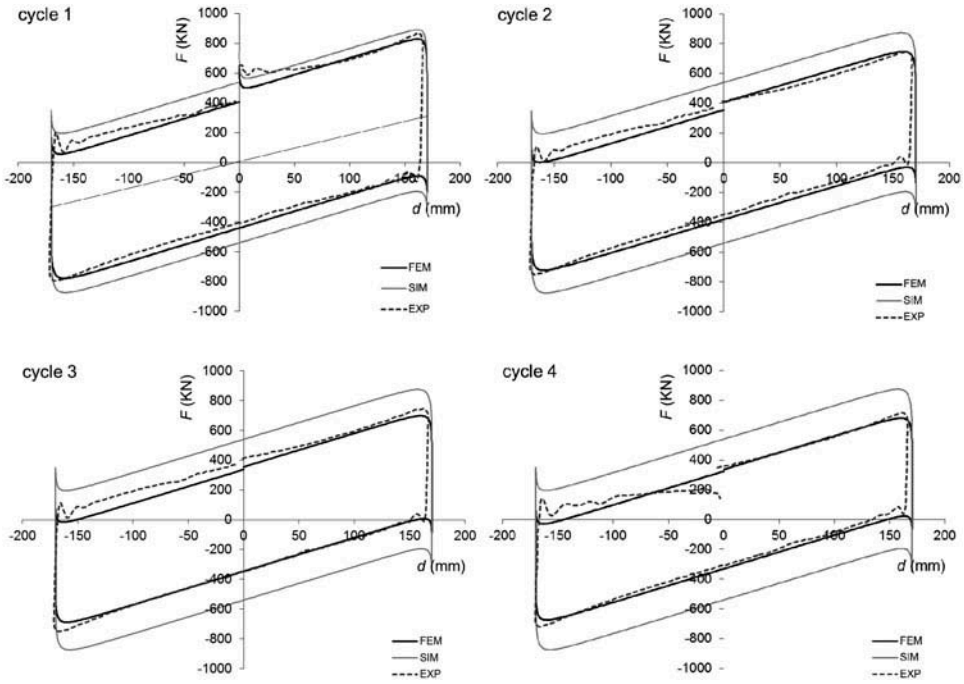

FIGURE 9 Hysteretic force–displacement curves of the CSS specimen in Test2. Experimental curves (EXP) compared to model predictions with either temperature–explicit (FEM) or temperature–independent simplified (SIM) friction formulation.

An isotropic friction model with three parameters representing the static and the kinetic coefficients of friction at either low or high velocity was coupled with a smooth temperature decay law defined by an exponential curve. Although rather simple, this model proved to well reproduce the experimental thermal-mechanical behavior of a real scale seismic isolator during uniaxial loading tests. The term $|sign(V) - sign(d)|$ introduced in Eq. (5) to account for the static coefficient of friction at motion starts is valid for cyclic displacement histories where stops occur only at cycle reversals. This assumption is realistic in general for seismic isolation systems subjected to either seismic shaking or to laboratory tests under applied cyclic loading, unless abnormal behavior like, e.g., stick-slip occurs [Hong and Liu, 2000].

The importance of the temperature-explicit formulation of coefficient of friction for an accurate prediction of temperature rise histories especially at high velocities is illustrated in Fig. 7. High flash temperatures developed in Test2 reduce the coefficient of friction and produce a substantial decrease in the heat generated at the interface, which in turn limits the further increase in temperature according to the mechanism of "thermal control of friction" [Ettles, 1986]. On the contrary, a friction formulation dependent on velocity only is not able to capture this mechanism and overestimates the actual temperature rise by feeding the model with a constant heat flux.

The temperature rise at the surface of the pad is a fundamental piece of information to assess the thermal stresses and the potential for wear of the bearing material. In contrast to conventional analytical solutions for thermal heating in the FPS based on the constant intensity heat source theory by Carslaw and Jaeger [1959], in the present approach the heat flux is an explicit function of local variables. The resulting temperature distribution is not

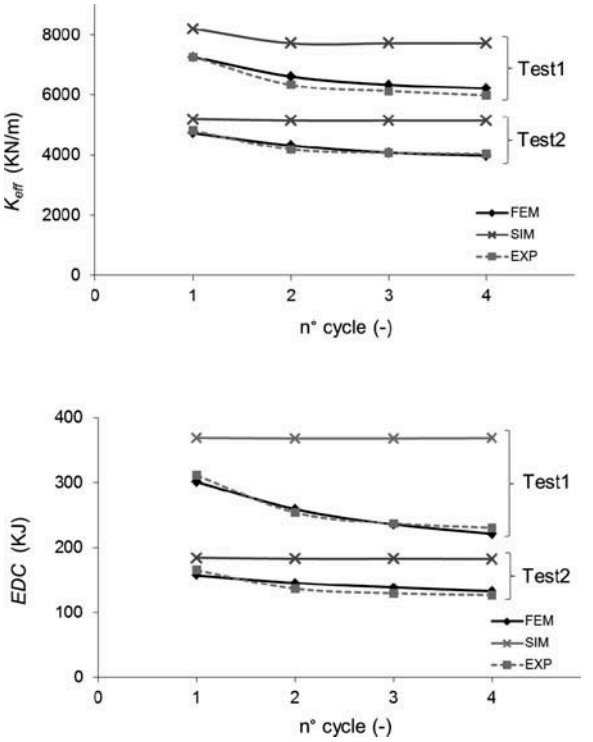

FIGURE 10 Effective stiffness (K_{eff}) and Energy Dissipated per Cycle (*EDC*) histories in Test1 and Test2. Experimental values (EXP) compared to model predictions with either temperature–explicit (FEM) or temperature–independent simplified (SIM) friction formulation.

uniform, and under the unidirectional loading histories considered in the analyses, peak values are attained close to the perimeter of the sliding pad perpendicularly to the direction of sliding. The areas of maximum temperature rise shift during the motion running nearly the whole span of the pad, and therefore a significant amount of the surface area of the bearing material is affected by high thermal stresses. The average surface temperature rise, as calculated in analytical procedures [Constantinou *et al.*, 2007], can lead to substantial underestimation of the actual peak flash temperatures, as shown in Table 6, and therefore of the potential (not uniform) wear of the material. It is also worth to note the huge discrepancy between the temperature rise at the thermocouple locations (on the back of the 2 mm thick

TABLE 6 Peak and average surface temperatures predicted in the temperature and velocity-explicit finite element analysis after four cycles of loading and temperature value recorded in laboratory tests at location of thermocouple TC5

	Temperature (°C)		
test (#)	peak	average	TC5
Test1	120.1	68.4	61.9
Test2	189.1	98.5	81.9

steel overlay) and at the surface of the sliding pad (Table 6); this fact should be considered when measurements of temperature are made by embedding thermocouples into the steel plates even if at small depths below the contact surface [Constantinou *et al.*, 2007; Wolff, 1999]. Another confirmation given by the finite element simulation is that owing to the low conductivity of the bearing material, frictional heating within the sliding pad is a local phenomenon affecting only the surface layers.

The numerical procedure has been used to predict the dynamic properties of the CSS unit under periodic loading. In order to avoid scale effects that are likely to affect the accuracy of friction properties measured on small scale specimens when extended to large scale analyses [Quaglini *et al.*, 2011], the parameters the friction model were calibrated directly on the force-displacement curves measured during the first cycle of motion of Test2. The agreement with the experimental curves is fair for all cycles of both Test2 and Test1, substantiating the accuracy of the proposed temperature–explicit friction formulation. The small gaps shown in Fig. 9 in the last branch of the cycle (from $d = -170$ mm to $d = 0$ mm) can be attributed indeed to the influence on the friction force of the vertical load fluctuations measured in the experiments (Fig. 2) rather than to the finite element formulation. Although these discrepancies have negligible effect on the accuracy of the predictions of stiffness and energy dissipation capacity of the isolator, it is necessary to underline that the accuracy of the numerical prediction depends on the testing data that are used to feed the subroutine of the finite element model.

Current standards [AASTHO, 2012; CEN, 2004] recommend property modification factors for the coefficient of friction of sliding surfaces to account for the change of the properties of bearings as a function of the minimum environmental temperature. It is acknowledged that at low temperature the coefficient of friction of thermoplastic materials increases, and the design values established in the standards are used in Upper Bound Analysis to calculate the maximum horizontal force developed by the bearing during non seismic movements.

As an effect of frictional heating, in presence of large friction forces and velocities the temperature at the sliding surface can rise to very high levels, producing a considerable decrease in the coefficient of friction that in turn affects the stiffness and damping capacity of the bearing. The minimum coefficient of friction occurring under seismic conditions shall therefore be considered in Lower Bound Analysis to evaluate the maximum bearing displacement occurring during the earthquake.

Sufficient background, either theoretical or experimental, on this subject is missing, and modification factors accounting for high temperatures related to seismic motions are not regulated yet. The assessment of the influence of frictional heating is today accounted for in the standards by prescribing cyclic tests on real scale specimens of the isolator: according to the European standard EN 15129 [2009], in 3 cycles of unidirectional loading up to the design displacement the maximum lateral force and the energy dissipated per cycle (*EDC*) shall deviate no more than 15% from their design values; ASCE/SEI 7-10 [2010] establishes a maximum deviation of the properties of the isolator of 20% over 10 cycles of loading, while the AASHTO Specification [2010] recommends a maximum variation of the effective stiffness and the *EDC* after 20 cycles of loading less than 20% and 30%, respectively. No prescription about the temperature resistance of the sliding materials is given. However assuming the maximum property variations recommended in the standards to establish the relevant modification factors for temperature increase during seismic loading is questionable, because these figures are relevant to friction variation in unidirectional tests and their validity under more general biaxial load patterns is not proven.

In the present study, only unidirectional loading histories performed in the laboratory tests on the CSS specimen were simulated in the analyses with the aim of providing

consistent numerical and experimental data. However thanks to the three-dimensional geometry of the model, the proposed numerical procedure has a more general validity and can be used to predict the response of CSS units under arbitrary bidirectional horizontal seismic motions with varying axial load, like the real histories isolation bearings are subjected to during the earthquake shaking [Gandelli *et al.*, 2012, 2013].

6. Conclusions

This study investigates the thermal-mechanical response of a Curved Surface Slider isolator to cyclic loading through the implementation of a three-dimensional finite element model of the complete bearing. The analysis supports the following conclusions.

1. The temperature-dependent formulation of the coefficient of friction of the bearing material allows to capture the self-limiting mechanism of frictional heating and to provide realistic predictions of temperature histories under high speed motion.
2. The finite element formulation accounts for the dependence of the heat flux on local variables, allowing to assess not uniform temperature rise distributions on the sliding surface; on the contrary, the assumption of uniform surface temperature can lead to severely underestimate actual peak values;
3. The procedure predicts the change of the mechanical properties of the isolator during periodic loading, confirming that decrease in stiffness and dissipation capacity of sliding isolators during seismic shaking is a potential issue related to heating of the sliding surfaces.

The authors believe that the numerical procedure can find useful application for the execution of dynamic analyses under design earthquakes for the estimation of lower bound design properties of sliding isolation bearings due to the effects of frictional heating, as well as in assisting preliminary studies for the selection of bearing materials accounting for their thermal stability. In addition, the procedure can support laboratory testing of real scale isolators, providing numerical assessment of temperature rise histories at the interface of the isolator that cannot be directly measured in the experiment.

References

ABAQUS Standard User's Manual Version 6.13 [2013] Dassault Systèmes Simulia Corp., Providence, Rhode Island.

ASCE/SEI 7-10 [2010] *Minimum Design Loads for Buildings and Other Structures*, American Society of Civil Engineers ASCE, Reston, Virginia.

AASHTO [2010] *Guide Specifications for Seismic Isolation Design*, American Association of State Highway and Transportation Officials, Washington.

AASHTO [2012] *LRFD Bridge Construction Specifications*, American Association of State Highway and Transportation Officials, Washington.

Braun, C. [2009] "The sliding isolation pendulum – an improved recentring bridge bearing," *Steel Constructions* **2**, 203–206.

Calvi, G. M., Pavese, A., Ceresa, P., Dacarro, F., Lai, C. G., and Beltrami, C. [2005] *Design of a Large-scale Dynamic and Pseudo-Dynamic Testing Facility*, IUSS Press, Pavia, Italy.

Carslaw, H. S. and Jaeger, J. C. [1959] *Conduction of Heat in Solids*, Oxford University Press, London.

Clarke, C. S. J., Buchanan, R., and Efthymiou, M. [2005] "Structural platform solution for seismic arctic environments – Sakhalin II offshore facilities," *Proc. of Offshore Technology Conference*, Houston, Texas, paper OTC-17378-PP.

CEN 15129 [2009] *Antiseismic Devices*, Comité Européen de Normalisation, Brussels.

CEN 1337-2 [2004] *Structural Bearings. Part 2: Sliding Elements*, Comité Européen de Normalisation, Brussels.

Constantinou, M. C., Mokha, A., and Reinhorn, A. [1990] "Teflon bearings in base isolation. II: Modeling," *ASCE Journal of Structural Engineering* **116**, 455–474.

Constantinou, M. C., Tsopelas, P., Kim, Y.-S., and Okamoto, S. [1993] *NCEER-Taisei Corporation Research Program on Sliding Seismic Isolation Systems for Bridges: Experimental and Analytical Study of a Friction Pendulum System [FPS], Report NCEER-93-0020*, National Center for Earthquake Engineering Research, Buffalo.

Constantinou, M. C., Whittaker, A. S., Kalpakidis, Y., Fenz, D. M., and Warn, G. P. [2007] *Performance of Seismic Isolation Hardware under Service and Seismic Loading, Report MCEER-07-0012*, National Center for Earthquake Engineering Research, Buffalo, New York.

Dolce, M., Cardone, D., and Croatto, F. [2005] "Frictional behavior of steel-PTFE interfaces for seismic isolation," *Bulletin of Earthquake Engineering* **3**, 75–99.

Drozdov, Y. N., Nadein, V. A., Puchkov, V. N., and Puchkov, M. V. [2008] "Heat state of pendulum sliding bearings under seismic effects," *Journal of Friction and Wear* **29**, 265–270.

Ettles, C. M. MCC. [1986] "Polymer and elastomer friction in the thermal control regime," *ASLE Transactions* **30**, 149–159.

Gandelli, E., Dubini, P., Bocciarelli, M., and Quaglini, V. [2012] "Numerical assessment of the seismic performance of sliding pendulum isolators," *Proc. of the* 15^{th} *World Congress on Earthquake Engineering*, Lisbon, Portugal, Paper No. 1607, pp. 1–10 on CD-ROM.

Gandelli, E., Quaglini, V., Dubini, P., Bocciarelli, M., and Poggi, C. [2013] "Frictional heating in sliding seismic isolators," *Proc. of the* 15^{th} *Congress on Italian Association of Seismic Engineering (ANIDIS)*, Padua, Italy, Paper No. 1455, pp. 1–10 on CD-ROM.

Hong, H.-K. and Liu, C.-S [2000] "Coulomb friction oscillator: modelling and responses to harmonic loads and base excitations," *Journal of Sound and Vibration* **229**, 1171–1192.

Incropera, F. P., Dewitt, D. P., Bergman, T. L., and Lavine, A. S. [2006] *Fundamentals of Heat and Mass Transfer*, 6th ed., John Wiley and Sons, New York.

Lanese, I., Pavese, A., and Dacarro, F. [2012] "Development of software and hardware architecture for real-time dynamic hybrid testing and application to a base isolated structure," *Journal of Earthquake Engineering* **16**, 65–82.

Mokha, A. S., Constantinou, M. C., and Reinhorn, A. M. [1991] "Experimental study of friction-pendulum isolation system," *Journal of Structural Engineering* **117**, 1201–1217.

Mokha, A. S., Avin, N., Constantinou, M. C., and Zayas, V. [1996] "Seismic isolation retrofit of a large historical building," *Journal of Structural Engineering* **122**, 298–308.

Mosqueda, G., Whittaker, A. S., and Fenves, G. L. [2004] "Characterization and modeling of Friction Pendulum Bearings subjected to multiple components of excitation," *Journal of Structural Engineering* **130**, 433–442.

Quaglini, V., Dubini, P., and Poggi, C. [2012] "Experimental assessment of sliding materials for seismic isolation systems," *Bulletin of Earthquake Engineering* **10**, 717–740.

Quaglini, V. and Dubini, P. [2011] "Assessment of sliding materials for pendulum isolation bearings," *Proc. of the* 7^{th} *World Conference on Joints, Bearings and Seismic Systems for Concrete Structures*, Las Vegas, Nevada, pp. 1–42 on CD Rom.

Sartori, M. [2012] "Seismic protection of railway bridges with sliding pendulum and high friction special sliding materials," *Proc. of the* 15^{th} *World Congress on Earthquake Engineering*, Lisbon, Portugal, paper No. 2296, pp. 1–8 on CD Rom.

Stachowiak, G. W. and Batchelor, A. W. [2005] *Engineering Tribology*, Butteworth Heinemann, Melbourne.

Tsai, C. S., Chen, W.-S., Chiang, T.-C., and Chen, B.-J. [2006] "Component and shaking table tests for full-scale multiple friction pendulum system," *Earthquake Engineering and Structural Dynamics* **35**, 1653–1675.

Tsopelas, P. and Constantinou, M. C. [1994] *NCEER-Taisei Corporation Research Program on Sliding Seismic Isolation Systems for Bridges: Experimental and Analytical Study of a System Consisting of Sliding Bearings and Fluid Restoring Force/Damping Devices, Report NCEER-94-0014*, National Center for Earthquake Engineering Research, Buffalo, New York.

Zayas, V. A., Low, S. S., and Mahin, S. A. [1987] *The FPS Earthquake Protection System, Report No. 87-01*, Earthquake Engineering Research Center, Berkeley, California.

Zayas, V. A., Low, S. S., and Mahin, S. A. [1990] "A simple pendulum technique for achieving seismic isolation," *Earthquake Spectra* **6**, 317–333.

Wolff, E. D. [1999] "Frictional heating in sliding bearings and an experimental study of high friction materials," MS Thesis, University at Buffalo, Buffalo, New York.